Time Domain Optical Studies of Dynamics in Supercooled *o*-Terphenyl: Comparison to Mode Coupling Theory on Fast and Slow Time Scales

S. D. Gottke, David D. Brace, G. Hinze,† and M. D. Fayer*

Department of Chemistry, Stanford University, Stanford, California 94305

Received: August 15, 2000; In Final Form: October 31, 2000

Orientational relaxation of supercooled *o*-terphenyl (OTP) is studied over a wide range of temperatures and time scales using optical heterodyne detected optical Kerr effect techniques. A combination of experimental setups made it possible to study the dynamics for greater than six decades of time (100 fs to hundreds of nanoseconds). The complex shape of the data is analyzed in terms of power laws at intermediate times and an approximately exponential decay at long times. Most features of the relaxation curves are in accord with predictions of mode-coupling theory (MCT) for supercooled liquids. In particular, at long times the relaxation data show a temperature independent shape in the temperature regime 361−290 K. When plotted vs temperature, the long time decay constants scaled by a relationship given by MCT fall on a line as predicted and give a value of the MCT critical temperature, $T_c = 285$ K, in accord with literature values. On a faster time scale, the slowest of the power law decays has a temperature-independent exponent, which is also in agreement with the predictions of MCT. Detailed comparisons of the data to MCT "master curves" show excellent agreement at times >10 ps. However, the faster component of the data (<10 ps) somewhat deviates in a systematic manner from the ideal MCT predictions. The deviations are in contrast to recent experiments on salol,[1] in which the predictions of ideal MCT reproduced the temperature-dependent data down to T_c on all time scales. Comparisons of the OTP data to calculations based on extended MCT do not improve the agreement. It is noted that a portion of the data at intermediate times (faster than the slowest power law), 2 ps < t < 5 ps to 300 ps (depending on temperature) can be described by a power law with a temperature-dependent exponent.

I. Introduction

Supercooled liquids have drawn considerable attention as subjects of fundamental research and because of their practical significance. Glasses are common natural materials and are important man-made materials. The properties of glassy materials are determined in part by the dynamical properties of supercooled liquids as they approach the glass transition temperature, T_g. Supercooled liquids exist in the liquid state below the thermodynamic temperature for crystallization. Therefore, a supercooled liquid is not in thermodynamic equilibrium. Crystallization is kinetically inhibited, and consequently, the dynamics of molecules in supercooled liquids are key to understanding their nature. As a supercooled liquid is cooled further and further below the crystalline melting point, molecular dynamics span an increasingly broad range of time scales. Very fast dynamics continue to occur, but the slowest dynamics take place on exceedingly long time scales. At T_g, the slowest dynamics, which give rise to complete structural relaxation, are essentially infinitely slow, and the material becomes a disordered glassy solid.

The enormous slowing down of the complete structural relaxation with decreasing temperature is a characteristic feature of supercooled liquids. The increasingly long time scale associated with structural relaxation is seen in macroscopic observables, like viscosity[2] and long time diffusion,[3] as well as in microscopic properties, like density fluctuations[4] and orientational relaxation times.[1,5,6] The reduction in rates of processes in supercooled liquids has been described by a number of phenomenological theories.[7] However, because of the broad ranges of time and amplitude associated with the dynamics in supercooled liquids, a complete understanding remains elusive.

Mode coupling theory (MCT)[8,9] is able to treat dynamics in supercooled liquids over the necessary broad range of time scales, from picoseconds to the longest decay times associated with complete structural relaxation. Because MCT provides quantitative predictions of the relaxation behavior of supercooled liquids, it has been the focus of numerous experiments,[9−12] many of which deal with short times (nanoseconds to picoseconds) or high frequencies (gigahertz to terahertz). Only a few experimental methods, for example, dielectric spectroscopy[13,14] and dynamic light scattering,[15−19] can cover a broad dynamic range. Most of the experimental methods used to study fast dynamics are frequency domain techniques, although there have been laser-based time domain measurements in the picoseconds−nanoseconds region.[20,21] Some neutron scattering experiments permit acquisition of time domain data in the picoseconds region.[22] In principle, time domain and frequency domain experiments can yield the same information. However, in practice, different aspects of the dynamics can be emphasized by various experiments.[23] Recent optical heterodyne detected optical Kerr effect (OHD-OKE) experiments on the organic liquid salol investigated orientational relaxation over 8 decades of time (100 fs to 10 μs) and a wide range of temperatures.[1,6] These experiments provided very detailed tests of MCT. All aspects of the experiments were in quantitative agreement with ideal MCT down to $\sim T_c$, the MCT critical temperature. At T_c

* Corresponding author.
† Permanent address: Institut für Physikalische Chemie, Johannes Gutenberg-Universität, Welderweg 15, D-55099 Mainz, Germany.

10.1021/jp002949d CCC: $20.00
Published on Web 12/12/2000

and below, the data[1] did not agree with the predictions of either ideal[8,9] or extended[24] MCT.[1]

In this paper, OHD-OKE experiments on the fragile glass forming liquid ortho-terphenyl (OTP) are presented and compared to MCT. OTP has been studied extensively with a wide range of experimental techniques. While some of them deal only with the slow structural relaxation of the liquid, the finding of faster secondary processes has triggered many sophisticated experiments focusing on the dynamics at faster time scales. The β-process described in the classic work of Johari and Goldstein[25] is located in the kHz regime below T_g. However, most of the recent experiments, such as neutron scattering[26−28] and dynamic light scattering,[16,29] deal with faster dynamics in the gigahertz to terahertz regime.

While in principle frequency domain and time domain experiments yield the same information, a detailed comparison of the two approaches led to the conclusion that the time domain representation can have advantages for comparing experimental data to theoretical predictions of MCT.[23] Fast time domain data is accessible by neutron scattering. Aside from the recent experiments on salol,[1,6] most detailed time domain experiments have been used for times longer than nanoseconds.

In the data presented below, OTP dynamics are measured from ∼100 fs to 100 ns over a wide range of temperatures by using several experimental setups. The complex shape of the data is analyzed in terms of power laws at intermediate times and an approximately exponential decay at long times. Most features of the relaxation curves are in accord with predictions of mode-coupling theory (MCT) for supercooled liquids. In particular, at long times the relaxation data show a temperature-independent shape in the temperature regime 361−290 K. When plotted vs temperature, the long time decay constants scaled by a relationship given by MCT fall on a line as predicted and give a value of $T_c = 285$ K, in accord with literature values. On a faster time scale, the slowest of the power law decays has a temperature-independent exponent, which is also in agreement with the predictions of MCT. Detailed comparisons of the data to MCT "master curves" show excellent agreement for times >10 ps. However, the faster component of the data (<10 ps) deviates in a systematic manner to some extent from the predictions of ideal MCT. The deviations are in contrast to recent experiments on the supercooled salol,[1] in which it was found that down to T_c the predictions of ideal MCT reproduced the temperature-dependent data on all time scales. Comparisons of the OTP data to calculations based on extended MCT do not improve the agreement. Like the salol data, at intermediate times (faster than the slowest power law), 2 ps < t < 5 ps to 300 ps (depending on temperature) the relaxation can be described by a power law with a temperature-dependent exponent. At the lowest temperatures, $\sim T_c$, the power law is $\sim t^{-1}$. The shortest time scale portion of the data, <2 ps, is dominated by intramolecular vibrational oscillations induced by stimulated Raman scattering cause by the ultrashort (∼70 fs) excitation pulse.

II. Experimental Procedures

The optical heterodyne detected optical Kerr effect experiment is a type of nonresonant pump−probe measurement.[30,31] The excitation pulse creates an optical anisotropy in the sample. Using short pulses ≤70 fs, the corresponding large bandwidth is sufficient to excite an orientationally anisotropic distribution of librations by stimulated Raman scattering (an impulsive torque) that is on a background of the thermally excited isotropic librational distribution. Damping of the librations leaves behind a residual orientational anisotropy that decays by orientational relaxation.[32,33] If the pulse is longer, the bandwidth is too narrow to excite librations by stimulated Raman scattering. However, an anisotropy develops because the $\vec{E}$-field exerts a torque on the molecules in the liquid that are undergoing thermal orientational fluctuations. The torque produces a net alignment of the molecules along the direction of the $\vec{E}$-field. For either type of excitation, the decay of the induced anisotropy toward an isotropic distribution is monitored with an additional probe pulse. By delaying the probe pulse optically, delay times up to 12 ns can be achieved. For longer times a CW probe is utilized in conjunction with a fast photomultiplier tube and fast digital sampling.

Two different pump lasers were employed for the experiments. For the ultrafast dynamics, that is, times from tens of femtoseconds to 600 ps, a laser system consisting of a regeneratively amplified Ti:sapphire oscillator produced pulses at a repetition rate of 5 kHz with a center wavelength of 800 nm. By adjusting the grating pulse compressor, the pulse duration could be varied from <70 fs to 2 ps. The shortest time scale data were recorded with the shortest pulses. For data out to 600 ps, the signal-to-noise ratio was improved by increasing the pulse duration. Increasing the pulse duration puts a frequency chirp on the pulse. However, for the nonresonant OKE experiment, a chirp does not change the data. For the slower dynamics, t > 100 ps, a mode-locked Q-switched cavity dumped Nd:YAG laser (1.06 μm) with a pulse length of 90 ps and a repetition rate of 1 kHz was used. Probe pulses were beam split from the excitation pulse for measurements to 12 ns. In the Ti:sapphire system, the probe and pump pulses were the same color. In the Nd:YAG system, the probe pulse was doubled to 532 nm. For t > 12 ns, the Nd:YAG pump and a 10 mW 650 nm diode laser probe were used. Optical heterodyne detection of the optical Kerr effect signal was employed[30,31] by rotating the quarter-wave plate slightly and leaving the input and output polarizers crossed. Compared to homodyne detection, OHD detection provides better signal-to-noise ratios, and OHD detection yields a signal that is linear in the third-order dielectric susceptibility. The peak pulse power was limited to avoid damaging the sample and to ensure that the homodyne component of the signal was negligible.

Data sets were taken on the three systems: Ti:sapphire, Nd:YAG with delayed probe, and Nd:YAG with CW probe. The scans taken over various time ranges always overlapped substantially with the time range of the next slowest scan. The extensive overlap of the scans permitted the data sets to be merged by adjusting only the relative amplitudes so the overlap regions were coincident. Great care was taken to ensure that the different data sets were properly and unambiguously merged. Sufficient data were accumulated so that the signal-to-noise ratios in the data overlap regions were excellent. In many cases, it is not possible to discern where the segments were combined.

Great care was taken in the preparation of the samples. Sample cuvettes were cleaned with a distillation apparatus. OTP, obtained from Aldrich, was purified and filled in glass cuvettes by vacuum distillation. Temperature control was obtained using a constant flow cryostat or closed cycle refrigerator with temperature stability of ±0.1 K.

III. Experimental Results

A typical OHD-OKE supercooled OTP data set is shown in Figure 1. At short times, t < 2 ps, oscillations are superimposed on the decay. The oscillations displayed on a log plot appear to have a peculiar form. Once the oscillations damp, it is possible

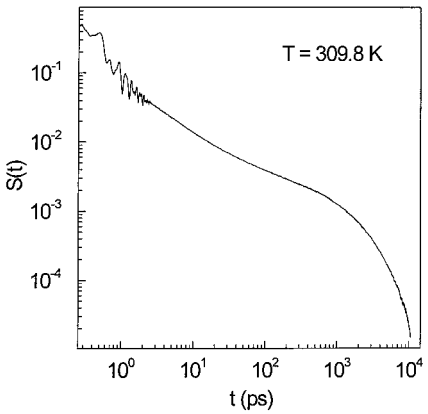

Figure 1. Heterodyne-detected optical Kerr effect data for the supercooled liquid OTP at 309.8 K. At the shortest times, $t < 2$ ps, oscillations originating from intramolecular vibrations dominate the signal. (The oscillations have a peculiar appearance because they are displayed on a log plot.) At longer times, the data consist of three regions. Two power laws can be identified with a crossover time at ~40 ps; at the longest times, the data decay is approximately exponential.

to discern different relaxation regions. The data has the appearance of a power law from ~2 to ~40 ps. Another power law appears to span the range of ~40 to 400 ps. After ~400 ps, the slowest, approximately exponential, portion of the data can be seen. These qualitative features can be seen at all of the temperatures that were studied.

The OHD-OKE signal, $S(t)$, is proportional to the third-order dielectric susceptibility.[34] However, a product of first-order dielectric tensors describes contributions arising from molecular motions, which are of interest here.[35] Hellwarth has given a detailed discussion of third-order dielectric susceptibilities and their relation to inelastic light scattering.[36] In the OHD-OKE experiment, an impulse response function is measured. With the appropriate selection of polarization conditions, $S(t)$ is directly related to the dynamic susceptibility $\chi''_{LS}(\omega)$ from depolarized light scattering.[35]

$$\chi''_{LS}(\omega) \propto \text{Im FT}\{S(t)\} \tag{1}$$

In depolarized light scattering, the measured intensity spectra, $I(\omega)$, must be divided by the Bose factor, which is essentially equivalent to $\chi''(\omega) \propto I(\omega) \times \omega$ for $\omega \leq 700$ GHz.[15] The OHD-OKE experiment yields the relevant information directly.

In Figure 2, the $S(t)$ data are plotted for a variety of temperatures measured in the range $284 \leq T \leq 361$ K. (The longest time portions of the low temperature data are not shown.) The figure shows the nature of the temperature dependence. The data are normalized at 300 fs, $S(t = 0.3 \text{ ps}) = 1$. For the 70 fs pulses used in the experiment, 300 fs is after the pulse shape and duration influence the form of the data. At all temperatures, the shapes of the data are qualitatively similar. The strongest temperature dependence is seen in the final portions of the decays at long times. At short times, $t < 2$ ps, the intramolecular vibrational oscillations are very pronounced, particularly at low temperatures.[1] The variation in this time regime with temperature can be attributed to the underlying decay. The oscillations were found to be temperature independent and consist of two frequencies with different amplitudes and damping rates (see Table 1). Once the oscillations are damped, the subsequent data can be decomposed into regions with different time dependences.

Figure 3 displays a portion of each data set. The data are shown for $t > 2$ ps but without the final long time decays. The

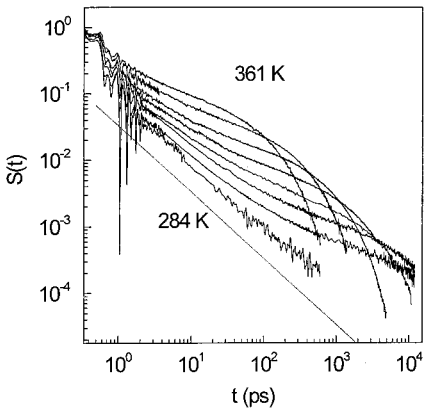

Figure 2. OHD-OKE data from OTP plotted for some of the temperatures measured to illustrate the temperature-dependent trends in the data. The temperatures are 284.0, 292.0, 296.0, 303.9, 309.8, 319.7, 334.5, and 361.0 K. The data were normalized at 300 fs. The slowest portions of the lowest temperature data sets are not shown. The data sets at each temperature have the same basic shape, but as the temperature is lowered, the time span of the data expands. The dashed line representing a t^{-1} power law is plotted as an aid to the eye.

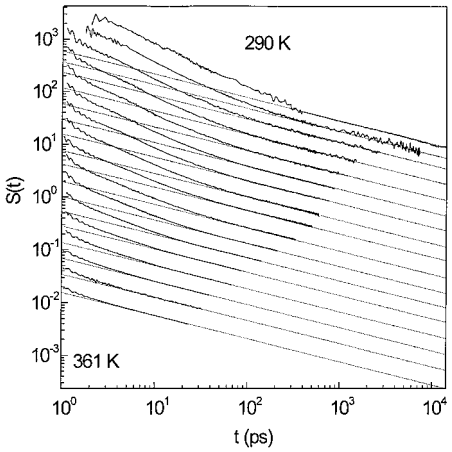

Figure 3. Intermediate time portion of the data from ~2 ps out to the onset of the approximately exponential decay shown for temperatures: 290.0, 292.0, 296.0, 298.0, 300.0, 302.0, 303.9, 305.0, 309.8, 311.0, 313.6, 319.7, 329.6, 334.5, 346.7, 351.0, and 361.0 K. For comparison, a power law with an exponent $p_1 = -0.44$ is shown (dotted line) with each data set. The data sets have been displaced along the vertical axis for clarity of presentation. The longer time portion of the data sets all have the same power law decay.

TABLE 1: Initial Oscillatory Part of the OHD-OKE Signal Decomposed into Two Components that Differ in Frequency, Amplitude, and Decay Time

	relative amplitude (%)	frequency (THz)	decay time (ps)
1	10	7.2	1.3
2	90	4.3	0.4

data sets are displaced along the vertical axis for clarity of presentation. The dotted lines all have the identical slope. The long time portion of each of the data sets falls on the dotted line. On a log plot, a straight line corresponds to a power law. At the highest temperatures, the data are almost described by this single line. However, at lower temperatures, there is clearly a change of form; the shorter time portions of the data also appear to be power laws. The shorter time portions of the data have temperature-dependent slopes on the log plot. The long time power law exponents, obtained via a least-squares fit, are plotted in Figure 4. While there is some variation because of

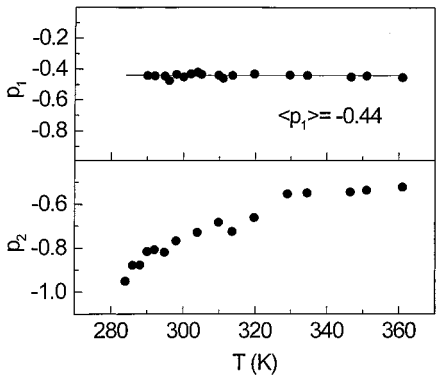

Figure 4. Power law exponents, p_1 and p_2, from the data sets in Figure 3. p_1, the longer time scale power law exponent, is temperature independent, while p_2, the power law exponent found at shorter times, displays a significant temperature dependence.

experimental error, the exponents are virtually identical. The slow power law exponent is temperature independent over the entire temperature range studied. The average of the slow power law exponents is $\langle p_1 \rangle = -0.44$. The line -0.44 is shown in the figure. The faster time scale portion of the curve can also be fit to a power law with an exponent that varies significantly with temperature. Similar behavior was found in the glass-forming liquid salol[6,1] (see below).

Following the slower power law, long time decay in supercooled liquids is attributed to final, complete structural relaxation. The slowest decay process is frequently referred to as the α-process. In the frequency domain, a Cole−Davidson distribution is often used to model the corresponding peak in the susceptibility.[14] In the time domain, a stretched exponential function, $\exp(-(t/\tau_\alpha)^\beta)$, is commonly employed to fit the long time scale data obtained using different experimental methods.[16,37,38] The main property of these functions is the strong asymmetry with regard to the frequency or time. The OHD-OKE experiment measures the time derivative of the polarizability−polarizability correlation function. Therefore, the longest time decay might be described by the derivative of a stretched exponential. The time derivative of a stretched exponential is proportional to a power law times the stretched exponential, that is

$$\propto t^{\beta-1} e^{-(t/\tau_\alpha)\beta}$$

In analyzing the OTP data, it was found that a simpler functional form is sufficient to fit the data

$$S(t) \propto t^p e^{-t/\tau_\alpha} \tag{2a}$$

Equation 2a is the time derivative of the long time (subscript L) portion of the correlation function, $\Phi_L(t)$. The correlation function is found by integrating the right-hand side of eq 2a to give $f(t)$, determining the constant of integration by the boundary condition that $\Phi_L(t) \rightarrow 0$ as $t \rightarrow \infty$, and normalizing the correlation function at $t = 0$ to 1. The result is

$$\Phi_L(t) = 1 - f'(t) \tag{2b}$$

where $f'(t)$ is $f(t)$ multiplied by the $t = 0$ normalization constant. $f'(t)$ is zero at $t = 0$ and 1 at $t = \infty$. $f(t)$ can be written as the incomplete gamma function

$$f(t) = \gamma(p + 1, t/\tau_\alpha)$$

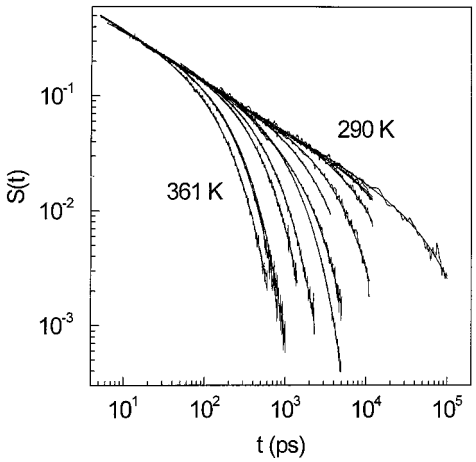

Figure 5. Long time portion of the data shown for $T \geq 290$ K. Fits to the data with $S(t) \propto t^p e^{-t/\tau_\alpha}$ are plotted as solid lines. The exponent p is temperature independent. τ_α, the structural relaxation decay constant, is highly temperature dependent. The fitting function has the correct functional form at all temperatures.

$\Phi_L(t)$ corresponds to the correlation function for the long time portion of the decay. The OTP data are fit with eq 2a using a temperature-independent value of p. Within experimental error, the value is approximately p_1 found in Figure 4. However, because of the influence of the exponential term, p is somewhat different from p_1. The average value of p is -0.38. The quality of the fits can be seen in Figure 5. Fitting with eq 2a leads to a well-defined relaxation time τ_α. The temperature-independent power law exponent p found in fitting the data means that the functional form (stretching) of the α process is temperature independent. The scaling of the correlation function $\Phi_L(t)$ for different values of τ_α can be demonstrated analytically.

IV. Comparison to Mode Coupling Theory

A. Ideal MCT. Mode coupling theory (MCT) makes quantitative predictions about dynamics in supercooled liquids.[8,9] In MCT, the fundamental dynamical quantity is the density−density correlation function $\Phi_q(t)$. In ideal MCT, a critical temperature, T_c, is associated with a dynamical phase transition from ergodic liquid dynamics to nonergodic glass dynamics below T_c. In real molecular liquids, structural relaxation occurs even below T_c, demonstrating a failing of the theory in its idealized form. However, even with this weakness, some predictions of ideal MCT are in accord with observations made on supercooled liquids[1,9] above T_c. (In many supercooled liquids, T_c is found to be $\sim 1.2\ T_g$.)

Two time scales, t_σ and τ_α, which follow characteristic scaling laws, describe the slowing down of dynamics as the temperature is reduced. t_σ is a rescaling time determined by a microscopic time t_0

$$t_\sigma = t_0 |\sigma|^{-1/2a} \tag{3}$$

with

$$\sigma = (T_c - T)/T_c \tag{4}$$

$$\tau_\alpha \propto |\sigma|^{-\gamma} \qquad \gamma = \frac{1}{2a} + \frac{1}{2b} \tag{5}$$

The exponent parameter λ is related to both a and b via

$$\lambda = \Gamma^2(1 - a)/\Gamma(1 - 2a) = \Gamma^2(1 + b)/\Gamma(1 + 2b) \tag{6}$$

where $\Gamma(x)$ is the complete gamma function. The temperature dependence is contained in σ. MCT predicts that the exponent, a, falls in the range $0 \leq a \leq 0.395$ and b falls in the range $0 \leq b \leq 1$.

While MCT deals directly with density fluctuations, many experimental methods, including OHD-OKE, probe orientational relaxation. There is considerable evidence that MCT also applies to other correlation functions (observables) that are coupled to density fluctuations.[8,9] The remarkable agreement with ideal MCT found in the orientational relaxation studies of salol strongly supports this argument.[1] While MCT originally treated hard spheres, which do not have orientational degrees of freedom, an extension including anisotropic interactions was published recently.[39,40]

The experimental OHD-OKE data were analyzed in section III for $t > 2$ ps by fitting to power laws with an approximately exponential decay (eq 2a) at long times. In MCT, the first scaling law (eq 3), called the β-relaxation regime, is located between the short (microscopic) time (~1 ps) and the α-relaxation time τ_α. In this regime the correlation function, $\Phi_q(t)$, is given by

$$\Phi_q(t) = f_q^c + h_q|\sigma|^{1/2} g_\lambda(t/t_\sigma) \qquad (7)$$

f_q^c is the critical Debye−Waller factor, and h_q is the critical amplitude. Above, but close to T_c, the scaling function g_λ is fully determined by the exponent parameter λ, and its shape is independent of temperature; that is, the curve is given by a temperature-dependent scaling relation. In first order, g_λ is given at short times, $t \ll t_\sigma$, by the critical decay power law[8,9]

$$g_\lambda = (t/t_\sigma)^{-a} \qquad (8)$$

while at longer times, $t \gg t_\sigma$, it is given by the von Schweidler power law

$$g_\lambda = -B(t/t_\sigma)^b \qquad B > 0 \qquad (9)$$

which describes the onset of the structural relaxation.

Identifying p_1 of Figure 4 in terms of the von Schweidler exponent yields $b = 1 + p_1 = 0.56$, since the OHD-OKE data are the derivative of the correlation function. This value of b leads to $a = 0.30$ and $\lambda = 0.75$. The critical decay power law should occur at very short times (<2 ps). The substantial amplitude of the high-frequency oscillations in the data on this time scale masks this region of the data (see <2 ps portion of Figure 2). (Use of 300 fs pulses eliminates the oscillations because the bandwidth of the pulse is too small to excite them. However, the very large electronic response obscures the data to times >2 ps. Therefore, increasing the pulse duration did not provide a method for elucidating the data at times <2 ps.) As discussed below, the power law exponent, p_2, shown in Figure 4, is not associated with a. It occurs at longer times, and it is temperature dependent.

First, consider the longest time scale behavior of the data, the α relaxation. Equation 5 describes the temperature dependence of τ_α. There are no adjustable parameters because γ is determined from the von Schweidler exponent b (Figure 4). Figure 6 displays τ_α as a function of temperature and the MCT predicted curve. The inset displays a so-called rectification diagram, which is $\tau_\alpha^{-1/\gamma}$ plotted vs the temperature. From the ideal MCT scaling relationship, the points should fall on a line. The intercept with the horizontal axis gives T_c. The results yield $T_c = 285$ K, in accord with previously reported values,[28,29] which have significant error bars. Figure 6 shows that the predictions of ideal MCT for the longest time scale dynamics are in excellent agreement with the experimental data. In addition, for the correlation function, $\Phi_L(t)$ that is obtained from integrating the fitting function, shape is independent of τ_α, as required by MCT.

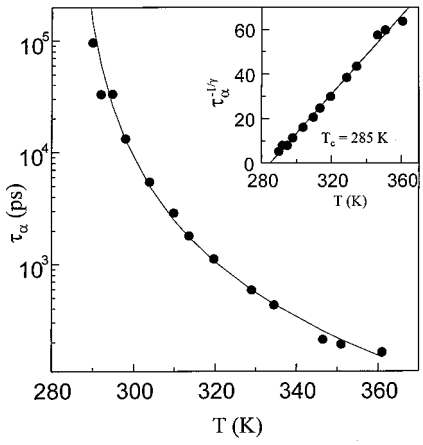

Figure 6. Structural relaxation exponential decay constant, τ_α, plotted vs temperature. The solid line through the data is obtained from the MCT scaling relationship (eq 5) with no adjustable parameters. The inset is the "rectification diagram". The points fall on a line as predicted by MCT and give a value of $T_c = 285$ K from the intercept on the x-axis.

In MCT, the next faster component of the data corresponds to the von Schweidler power law. As shown in Figure 3, the data are indeed a power law, and as predicted by MCT. Consistent with MCT, the power law exponent, b, is temperature independent (see Figure 4, $b = 1 + p_1 = 0.56$). Thus, ideal MCT properly describes the moderately fast dynamics. The results obtained here are in contrast to previously reported light scattering results that were fit with a temperature-dependent b.[29] The value of b obtained in this work falls within the range of the values obtained from the light scattering experiments.

Both the critical decay power law and the von Schweidler power law (eqs 8 and 9) are the leading terms of the power law expansion[41,42] of the full correlation function on time scales fast compared to the α-relaxation.[43] The correlation function, or its power law expansion, describes a master curve that has a definite scaling behavior with temperature. In Figure 7, the experimental data are compared to the master curves calculated with ideal MCT, including higher order terms.[42] The theoretical curves were generated by employing the power law expansion with the appropriate coefficients[41,42] for $\lambda = 0.75$. In the data, the shortest time portions have oscillations.

For the highest three temperatures in Figure 7, the master curves appear to work quite well. However, at lower temperatures, there are deviations between the data and the calculations at the shorter times, $t < 10$ ps, that are well beyond experimental error. The deviations have a particular temperature-dependent character. At the higher temperatures, the data falls above the calculated curves. At $T = 313.6$ (7th curve from the bottom), the data again appear to fall on the master curve. However, at still lower temperatures, the data fall below the master curves. Thus, the sense of the deviation changes. By 290 K, the deviation is quite large. These deviations are in contrast to previously reported results on salol.[1] OHD-OKE experiments on salol show excellent agreement between the master curve and the data on all time scales for $t > 2$ ps until the temperature is reduced close to T_c. At T_c, ideal MCT predicts a plateau (structural relaxation at long time is incomplete), which is not observed. The data are continuous in nature through T_c. Therefore, the predictions of ideal MCT will fail at ~T_c. The

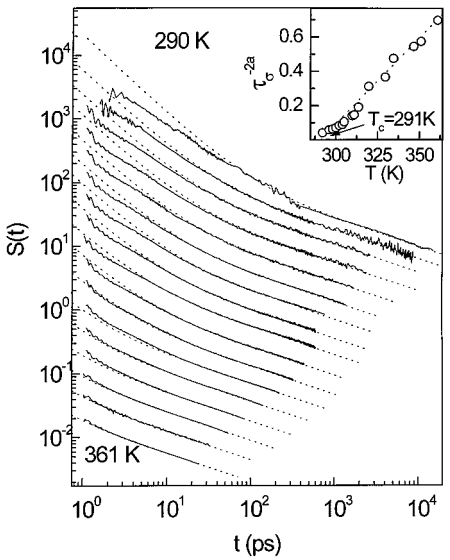

Figure 7. Data and ideal MCT master curve calculations. (The temperatures are the same as those listed in the caption of Figure 3.) The data do not include the long time portion analyzed in Figure 6. The master curves are calculated with no adjustable parameters. The calculated curves agree with the data at the three highest temperatures and at all temperatures at longer times. However, at the lower temperatures at short times (<10 ps), there are deviations between the data sets and the calculated curves. The inset shows the "rectification diagram." While the points have considerable scatter, they appear to have the predicted linear dependence on temperature, and give a value of $T_c = 291$ K, which is in accord with the determination of T_c in Figure 6 and with literature values, within experimental error.

largest deviation in the OTP data occurs at 290 K, which is $\sim T_c$. This large deviation between the master curve and the data probably occurs because $T \cong T_c$. At the higher temperatures, in the critical decay region, $t \ll t_\sigma$, systematic deviations between data and theory are found which are not due to the proximity of the temperature to T_c.

The rectification diagram, t_σ^{-2a} vs temperature, is plotted in the inset of Figure 7. MCT predicts that the points should fall on a line. While there is considerable scatter in the data, a linear fit gives $T_c = 291$ K, which is somewhat higher than the value determined from the better quality data shown in the inset in Figure 6. Both values are within the range of values (~290 K) reported previously.[28,29]

B. Extended MCT. In the extended version of MCT, a "hopping term" is added to the equation of motion to restore ergodicity below T_c.[24] In idealized MCT, the structural relaxation time τ_α diverges at T_c, while in the extended MCT the activated hopping process permits full relaxation even at $T < T_c$. In ideal MCT, T_c would be the glass transition temperature. Extended MCT accounts for the experimental fact that $T_g < T_c$. The addition of the hopping term affects the correlation function g_λ, which is no longer temperature independent.[24] Rather, g_λ becomes a function of T, λ and δ, where δ is the hopping parameter. δ and $\sigma = (T_c - T)/T_c$ can be combined with the microscopic time t_0 to give $\hat{\delta} = t_0\delta/\sigma$. $\hat{\delta}$ corresponds to ideal MCT. The reports of an experimental "knee" in the frequency domain susceptibility $\chi''(\omega)$ were used to support the introduction of the hopping process. However, recent improvements in light scattering experiments have identified the knee as an experimental artifact.[44−46]

In Figure 8, several extended MCT calculations and a data set are plotted. The calculations include small and large hopping contributions. A direct comparison shows that neither case is compatible with the experimental data; rather, the curve that

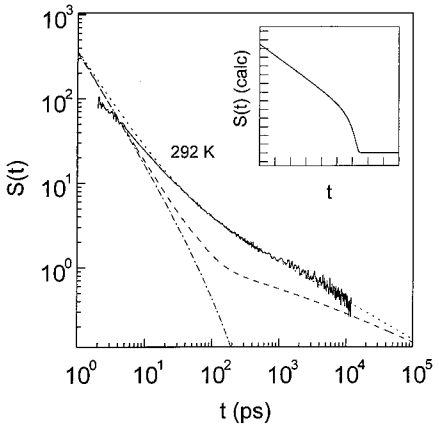

Figure 8. Experimental data at 292 K and extended MCT calculations with $\lambda = 0.75$ for three cases: (a) $\hat{\delta} = 0$, no hopping (dotted line), (b) $\hat{\delta} \gg 1$, substantial hopping (dashed line), and (c) $\hat{\delta} \ll 1$, relatively little hopping (dashed−dotted line). All other calculations performed for a wide range of parameters produce curves that fall between those shown. The calculations show that extended MCT cannot account for the shape of the experimental data below T_c. The impulse response function for case (c) ($\hat{\delta} \ll 1$) shows an additional feature following the critical decay; the relaxation first slows down and then speeds up again at longer times. A typical example is plotted against log t (10^{-5}−10^4 ps) in the inset with $\hat{\delta} = 10^{-6}$. The vertical position of the plateau, which appears after the downward bend, depends on the value of $\hat{\delta}$.

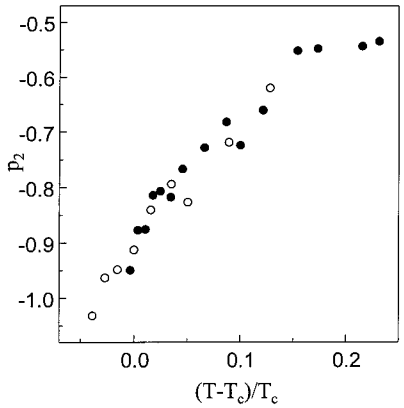

Figure 9. Temperature-dependent intermediate power law exponent, p_2, is shown for both OTP (filled circles) and salol (open circles).[1,6] The data are plotted vs a reduced temperature, $(T - T_c)/T_c$. Within experimental error, the intermediate power law has the same temperature dependence in the two liquids.

comes closest to the data is for $\hat{\delta} = 0$, which corresponds to ideal MCT. Calculations were performed that spanned a wide range of extended MCT parameters. All of the curves fell between the ones shown in Figure 8. None of them matched the data. Independent of the choice of $\hat{\delta}$, the decay calculated with extended MCT falls too quickly at $t \sim t_\sigma$.

C. Intermediate Power Law. As discussed above, MCT master curves show some deviations from the data at short times (t < 10 ps) although ideal MCT does an excellent job of describing the salol data on all time scales down to T_c.[1] In both OTP and salol,[1,6] the intermediate time scale data are well described by a power law with a temperature-dependent exponent. For OTP, this exponent is p_2 given in Figure 4. The temperature-dependent behavior of this "intermediate" power law in OTP and salol are very similar. Figure 9 shows the intermediate power law exponents vs a reduced temperature for both OTP and salol, in the case of OTP using a value of $T_c = 285$ K. At high temperature, the exponents are ~−0.6 and decrease to ~−1 at ~T_c. The dotted line in Figure 2 is $a\ t^{-1}$

power law. The intermediate power law falls between the fast critical decay power law and the von Schweidler power law. Within experimental error, the two liquids display identical temperature-dependent intermediate power law exponents when plotted against the reduced temperature. In some sense, this power law may simply reflect the intermediate time portion of the MCT master curve. However, unlike the master curve, the data do not have a discontinuity at T_c, and it is interesting that the reduced temperature dependences for the two liquids are the same. Near T_c, the exponent is ~ -1, which could correspond to $1/f$ noise in the spectral density or a logarithmic decay of the correlation function $\Phi(t)$, which would result in a power law decay of the OHD-OKE data with exponent -1.

The scaling functions, $g_\lambda(t/t_\sigma)$, used above are the predictions of MCT from the leading asymptotic behavior of the time and the temperature dependence of a generic correlation function. Recently, the next order corrections to the asymptotic solutions were calculated.[23] They yield a wave vector dependence of $g_\lambda(t/t_\sigma)$ for both the critical decay and the von Schweidler regime. The calculations involve the translational degrees of freedom, that is, density fluctuations. Although the equivalent results are not known for orientational relaxation, the calculated corrections are temperature independent, which would seem to exclude this modification of $g_\lambda(t/t_\sigma)$ as an explanation for the experimentally observed temperature dependence of the intermediate power law exponent p_2.

A detailed study of the translational−rotational correlation function for a system of diatomic and rigid molecules interacting via a Lennard-Jones potential has been performed recently using molecular dynamics simulation.[48,49] A principal result concerning the MCT predictions is the existence of a single transition temperature T_c for all correlation functions. Furthermore, it was found that the density−density correlation function and the second Legendre polynomial orientational correlation function, which describes OHD-OKE experiments, behaved in the same manner; they follow the universal time dependence of the critical correlation function $g_\lambda(t/t_\sigma)$. In addition, a theoretical extension of MCT to molecular liquids of nonspherical particles was developed recently.[50] The findings support the applicability of MCT to OHD-OKE data and indicate that the temperature-dependent intermediate power law observed in the experiments on OTP and salol do not arise because of the nature of the observable.

V. Concluding Remarks

Time domain experiments covering a broad range of time scales on the glass-forming liquid OTP have explored the dynamics in the supercooled state down to the MCT transition temperature, T_c. The experiments employing optical heterodyne detected optical Kerr effect were able to span a time range from $\sim$100 fs to $\sim$100 ns. The data have a complex shape, ranging from high-frequency intramolecular oscillations at short times to approximately exponential relaxation at long times.

Several features predicted by idealized mode-coupling theory are in accord with the OTP data. The longest time scale structural relaxation (α relaxation) obeys the scaling predictions of MCT. The observation of a temperature-independent power law (the von Schweidler power law) at times somewhat faster than the α relaxation is also in agreement with MCT. The scaling time, t_σ shows the predicted MCT behavior. The MCT master curve calculations show good agreement with the data except at short times. At short times ($t < 10$ ps), there are small but systematic deviations between the master curves and the data. Using extended MCT, calculations including a hopping process do not improve the agreement. The inability of the ideal MCT master curve to reproduce the OTP data down to T_c is in contrast to recent experiments on salol.[1] In the salol experiments, it was found that the predictions of ideal MCT were in remarkable agreement with the data on all time scales and at all temperatures down to $\sim T_c$.

Overall, the agreement between ideal MCT predictions and the OTP data is substantial. It is unclear at this time why ideal MCT shows deviations from the OTP data in the critical decay region but shows agreement with the salol data. It has been argued that at very short time times, some form of "microscopic dynamics" extend into the longer time scale of the critical behavior[51] and, therefore, distort the appearance of the critical decay. The Boson peak[52] is one such microscopic phenomenon that is not part of MCT and may contribute to the signal in the ps regime. Although a comparison of OTP and salol with light scattering showed that the Boson peak is somewhat larger in OTP, the difference in intensities is not large.[53] For the OHD-OKE experiments presented on OTP and salol, it is not clear why the Boson peak might influence the data in one system and not the other.

Another possible explanation for the observed differences on fast times scales between OTP and salol is in the actual nature of the two liquids. OTP is a somewhat more fragile[52] glass forming liquid than salol. OTP is virtually nonpolar and cannot form hydrogen bonds. Salol is polar and has the potential to form intermolecular hydrogen bonds. It will be important in future experiments on other liquids to determine if such differences play a role in the extent of quantitative agreement between data and MCT.

Acknowledgment. We would like to thank Professor H. C. Andersen, Department of Chemistry, Stanford University, for informative conversations pertaining to this work. We thank A. Latz, Department of Physics, University of Mainz, for providing considerable help and computer software used to perform the extended MCT calculations. We also thank Hu Cang, Department of Chemistry, Stanford University, for some analysis used in this work. This research was made possible by a grant from the National Science Foundation (DMR-0088942). G.H. would like to thank the Alexander von Humboldt Foundation for partial support.

References and Notes

(1) Hinze, G.; Brace, David D.; Gottke, S. D.; Fayer, M. D. *J. Chem. Phys.*, in press.
(2) Angell, C. A. *J. Phys. Chem. Solids* **1988**, *49*, 863.
(3) Chang, I.; Sillescu, H. *J. Phys. Chem.* **1997**, *101*, 8794.
(4) Götze, W.; Sjögren, L. *Rep. Prog. Phys.* **1992**, *55*, 241.
(5) Hinze, G.; Sillescu, H. *J. Chem. Phys.* **1996**, *104*, 314.
(6) Hinze, G.; Brace, David D.; Gottke, S. D.; Fayer, M. D. *Phys. Rev. Lett.* **2000**, *84*, 2437.
(7) Ediger, M. D.; Angell, C. A.; Nagel, S. R. *J. Phys. Chem.* **1996**, *100*, 13200.
(8) Götze, W.; Sjögren, L. *Rep. Prog. Phys.* **1992**, *55*, 241.
(9) Götze, W. *J. Phys.: Condens. Matter* **1999**, *11*, A1.
(10) Giordano, M.; Leponini, D.; Tosi, M. Second Workshop on Non-Equilibrium Phenomena in Super-Cooled fluids, Glasses, and Amorphous Materials. *J. Phys. Condens. Matter* **1999**, *11*, A1−A377.
(11) Ngai, K. L.; Riande, E.; Wright, G. B. Proceedings of the Second International Discussion Meeting on Relaxations in Complex Systems. *J. Non-Cryst. Solids* **1994**, *172−174*, 1−435.
(12) Ngai, K. L.; Riande, E. Proceedings of the Third International Discussion Meeting on Relaxations in Complex Systems. *J. Noncryst. Solids* **1998**, *235−237*, 1−800.
(13) Lunkenheimer, P.; Pimenov, A.; Dressel, M.; Goncharov, Y. G.; Böhmer, R.; Loidl, A. *Phys. Rev. Lett.* **1996**, *77*, 318.
(14) Schneider, U.; Lunkenheimer, P.; Brand, R.; Loidl, A. *Phys. Rev. E* **1999**, *59*, 6924.

(15) Li, G.; Du, W. M.; Chen, X. K.; Cummins, H. Z. *Phys. Rev. A* **1992**, *45*, 3867.
(16) Cummins, H. Z.; Li, G.; Du, W.; Hwang, Y. H.; Shen, G. Q. *Prog. Theor. Phys. Suppl.* **1997**, *126*, 21.
(17) Bergmann, R.; Börjesson, L.; Torell, L. M.; Fontana, A. *Phys. Rev. B* **1997**, *56*, 11619.
(18) Li, G.; Du, M.; Sakai, A.; Cummins, H. Z. *Phys. Rev. A* **1992**, *46*, 3343.
(19) Wuttke, J.; Goldammer, M. Submitted for publication.
(20) Torre, R.; Bartolini, P.; Pick, R. M. *Phys. Rev. E* **1998**, *57*, 1912.
(21) Sengupta, A.; Fayer, M. D. *J. Chem. Phys.* **1994**, *100*, 1673−1683.
(22) Petry, W.; Bartsch, E.; Fujara, F.; Kiebel, M.; Sillescu, H.; Farago, B. *Z. Phys. B−Condens. Matter* **1991**, *83*, 175.
(23) Franosch, T.; Fuchs, M.; Goetze, W.; Mayr, M. R.; Singh, A. P. *Phys. Rev. E* **1997**, *55*, 7153.
(24) Fuchs, M.; Götze, W.; Hildebrand, S.; Latz, A. *J. Phys.*: *Condens. Matter* **1992**, *4*, 7709.
(25) Johari, G. P.; Goldstein, M. *J. Chem. Phys.* **1970**, *53*, 2372.
(26) Tölle, A.; Fujara, F. Manuscript in preparation.
(27) Wuttke, J.; Kiebel, M.; Bartsch, E.; Fujara, F.; Petry, W.; Sillescu, H. *Z. Phys. B* **1993**, *91*, 357.
(28) Tölle, A.; Schober, H.; Wuttke, J.; Fujara, F. *Phys. Rev. E* **1997**, *56*, 809.
(29) Steffen, W.; Patkowski, A.; Gläser, H.; Meier, G.; Fischer, E. W. *Phys. Rev. E* **1994**, *49*, 2992.
(30) McMorrow, D.; Lotshaw, W. T.; Kenney-Wallace, G. *IEEE J. Quantum Electron.* **1988**, *24*, 443.
(31) McMorrow, D.; Lotshaw, W. T. *J. Phys. Chem.* **1991**, *95*, 10395.
(32) Ruhman, S.; Williams, L. R.; Joly, A. G.; Kohler, B.; Nelson, K. A. *J. Phys. Chem.* **1987**, *91*, 2237.
(33) Deeg, F. W.; Stankus, J. J.; Greenfield, S. R.; Newell, V. J.; Fayer, M. D. *J. Chem. Phys.* **1989**, *90*, 6893−6902.
(34) Ho, P. P.; Alfano, R. R. *Phys. Rev. A* **1979**, *20*, 2170.
(35) Kinoshita, S.; Kai, Y.; Yamaguchi, M.; Yagi, T. *Phys. Rev. Lett.* **1995**, *75*, 148.
(36) Hellwarth, R. W. *Prog. Quantum Electron.* **1977**, *5*, 1.
(37) Fuchs, M.; Hofacker, I.; Latz, A. *Phys. Rev. A* **1992**, *45*, 898.
(38) van Megen, W.; Underwood, S. M. *Phys. Rev. E* **1994**, *49*, 4206.
(39) Scheidsteger, T.; Schilling, R. *Philos. Mag. B* **1998**, *77*, 305.
(40) Fabbian, L.; Latz, A.; Schilling, R.; Sciortino, F.; Tartaglia, P.; Theis, C. *Phys. Rev. E* **1999**, *60*, 5768.
(41) Bartsch, E. *Transp. Theory Stat. Phys*. **1995**, *24*, 1125.
(42) Götze, W. *J. Phys.: Condens. Matter* **1990**, *2*, 8485.
(43) Li, G.; Fuchs, G. M.; Du, W. M.; Latz, A.; Tao, N. J.; Hernandez, J.; Götze, W.; Cummins, H. Z. *J. Non-Cryst. Solids* **1994**, *172*, 43.
(44) Surovtsev, N. V.; Wiedersich, J. A. H.; Novikov, V. N.; Rössler, E.; Sokolov, A. P. *Phys. Rev. B* **1998**, *58*, 14888.
(45) Barshilia, H. C.; Li, G.; Shen, G. Q.; Cummins, H. Z. *Phys. Rev. E* **1999**, *59*, 5625.
(46) Gapisnki, J.; Steffen, W.; Patkowski, A.; Sokolov, A. P.; Kisliuk, A.; Buchenau, U.; Russina, M.; Mezei, F.; H.; S. *J. Chem. Phys.* **1999**, *110*, 2312.
(47) Götze, W.; Haussmann, R. *Z. Phys. B−Condens. Matter* **1988**, *72*, 403.
(48) Kämmerer, S.; Kob, W.; Schilling, R. *Phys. Rev. E* **1997**, *56*, 5450.
(49) Kämmerer, S.; Kob, W.; Schilling, R. *Phys. Rev. E* **1998**, *58*, 2141.
(50) Schilling, R.; Scheidsteger, T. *Phys. Rev. E* **1997**, *56*, 2932.
(51) Sciortino, F.; Tartaglia, P. *J. Phys.: Condens. Matter* **1999**, *11*, 261.
(52) Sokolov, A. P.; Rössler, E.; Kisliuk, A.; Quitmann, D. *Phys. Rev. Lett.* **1993**, *71*, 2062.
(53) Sokolov, A. P.; Rössler, E.; Kisliuk, A.; Soltwisch, M.; Quitmann, D. *Physica A* **1993**, *201*, 67.